

# Mitochondrial remnant organelles of *Giardia* function in iron-sulphur protein maturation

Jorge Tovar<sup>1</sup>, Gloria León-Avila<sup>1</sup>, Lidya B Sánchez<sup>2\*</sup>, Robert Sutak<sup>3</sup>, Jan Tachezy<sup>3</sup>, Mark van der Giezen<sup>1</sup>, Manuel Hernández<sup>1</sup>, Miklós Müller<sup>2</sup> & John M. Lucocq<sup>4</sup>

<sup>1</sup>School of Biological Sciences, Royal Holloway, University of London, Egham, Surrey TW20 0EX, UK

<sup>2</sup>The Rockefeller University, 1230 York Avenue, New York, New York 10021, USA

<sup>3</sup>Department of Parasitology, Faculty of Science, Charles University, 12844 Prague 2, Czech Republic

<sup>4</sup>School of Life Sciences, WTB/MSI complex, University of Dundee, Dundee DD1 5EH, UK

\* Present address: Public Health Research Institute, Newark, New Jersey 07103, USA

*Giardia intestinalis* (syn. *lamblia*) is one of the most widespread intestinal protozoan pathogens worldwide, causing hundreds of thousands of cases of diarrhoea each year<sup>1</sup>. *Giardia* is a member of the diplomonads, often described as an ancient protist group whose primitive nature is suggested by the lack of typical eukaryotic organelles (for example, mitochondria, peroxisomes), the presence of a poorly developed endomembrane system and by their early branching in a number of gene phylogenies<sup>1,2</sup>. The discovery of nuclear genes of putative mitochondrial ancestry in *Giardia*<sup>3-7</sup> and the recent identification of mitochondrial remnant organelles in amitochondrial protists such as *Entamoeba histolytica*<sup>8,9</sup> and *Trachipleistophora hominis*<sup>10</sup> suggest that the eukaryotic amitochondrial state is not a primitive condition but is rather the result of reductive evolution. Using an *in vitro* protein reconstitution assay and specific antibodies against IscS and IscU—two mitochondrial marker proteins involved in iron-sulphur cluster biosynthesis—here we demonstrate that *Giardia*

contains mitochondrial remnant organelles (mitosomes) bounded by double membranes that function in iron-sulphur protein maturation. Our results indicate that *Giardia* is not primitively amitochondrial and that it has retained a functional organelle derived from the original mitochondrial endosymbiont.

The assembly and maturation of iron-sulphur (Fe-S) proteins is a recently identified critical function of the mitochondrion<sup>11</sup>. Proteins containing Fe-S centres are widely distributed in nature and operate in metalloenzyme catalysis and electron transport. Although several Fe-S proteins are important in energy metabolism in amitochondriate organisms (for example, pyruvate:ferredoxin oxidoreductase, ferredoxin, hydrogenase)<sup>12</sup>, almost nothing is known about the maturation of these proteins into functional enzymes or about the biosynthesis of their essential Fe-S reactive centres. Genes encoding the soluble enzyme cysteine desulphurase (IscS), a central component of the Fe-S cluster assembly system of prokaryotic and eukaryotic cells, were recently cloned from the amitochondrial protists *Trichomonas vaginalis* and *Giardia intestinalis*<sup>5</sup>. Because phylogenetic analyses of these genes support their mitochondrial ancestry, it is possible that their encoded proteins are still compartmentalized into a mitochondrion-derived organelle. While the mitochondrion-related hydrogenosome of *Trichomonas* is a good candidate for this function<sup>13,14</sup>, a mitochondrion-derived intracellular compartment in *Giardia* has not been identified, despite mounting evidence suggesting its existence<sup>3-7,15,16</sup>.

We cloned and characterized a second *Giardia* gene involved in the biosynthesis of Fe-S clusters, the *GiiscU* gene. This gene encodes the soluble iron-binding protein IscU, a functional partner of IscS thought to participate as a scaffold protein that forms Fe-S molecular complexes in conjunction with IscS (ref. 11). Amino acid sequence comparison of the *Giardia* IscU with bacterial and eukaryotic homologues revealed a high degree of similarity along the entire length of the protein (63–69% similarity, 46–51% identity), with conservation of cysteine residues essential for *in vivo* functionality<sup>17</sup>. Similar to IscS (ref. 5), phylogenetic analyses provide significant support for the clustering of *Giardia* IscU with

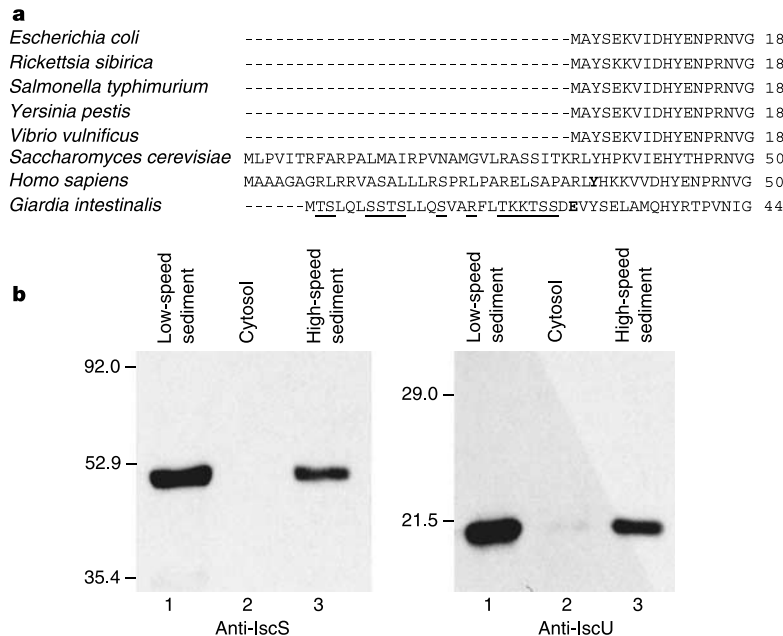


**Figure 1** Distribution of IscU and IscS in *Giardia* cell extracts. **a**, Comparison of N-terminal regions of prokaryotic and eukaryotic IscU proteins aligned by CLUSTALW. Hydroxylated and basic amino acids of the *Giardia* sequence are underlined. E27, the proposed N-terminal cleavage site of the *Giardia* sequence and Y35, the first residue of the mature

human IscU (ref. 18), are in bold typeface. **b**, Distribution of Isc proteins in *Giardia* fractions obtained by differential centrifugation. Trophozoite extracts fractionated as described in Methods were electrophoresed, blotted and probed with specific antibodies against IscS and IscU. Sizes of molecular markers are given in kDa.

mitochondrial homologues (not shown). The amino-terminal sequence of IscU is rich in hydroxylated and basic amino acids reminiscent of mitochondrial-targeting presequences (Fig. 1a). Analysis of this sequence using MitoProt predicts the mitochondrial localization of *Giardia* IscU with high confidence ( $P > 0.95$ ). The predicted N-terminal cleavage site at E27 coincides with the first amino acid residue of all prokaryotic IscU sequences and is two residues upstream of Y35, the cleavage site of the human sequence<sup>18</sup>. These findings suggest that the N-terminal sequence might target IscU to a mitochondrion-derived organelle in this organism.

To test this hypothesis we overexpressed *Giardia* IscU and IscS in *Escherichia coli* and generated antibodies against the recombinant proteins. The specific anti-IscU and anti-IscS antibodies were used for immunoblotting of subcellular fractions obtained by differential centrifugation. Protein bands of around 49 and 19 kDa were identified, in good agreement with the sizes of IscS and IscU respectively, predicted from their genomic sequences. Both proteins were found predominantly in the low-speed sediment of unbroken cells and cell debris (see Methods for details) and in the high-speed pellet containing sedimentable particulate matter such as membranes and membrane-bounded organelles (Fig. 1b, lanes 1 and 3). Little or no label was found in the cytosol, suggesting that both proteins are compartmentalized in this organism.

We tested the functionality of *Giardia* Fe-S protein maturation using an *in vitro* reconstitution assay that monitors the assembly of *de novo* synthesized radiolabelled Fe-S clusters into recombinant ferredoxin apoprotein lacking Fe-S moieties. Formation of fully assembled ferredoxin occurs exclusively when the high-speed sediment is used in the reaction (Fig. 2). Incubation with cytosolic proteins did not produce significant incorporation of label into ferredoxin and the addition of EDTA, a metal chelator, completely inhibited ferredoxin maturation. These results are consistent with the observed cellular distribution of Isc proteins in *Giardia* and demonstrate that Fe-S cluster biosynthesis, a mitochondrial biosynthetic pathway, is fully operational in this amitochondrial organism.

The compartmentalized distribution of IscS and IscU in *Giardia* was demonstrated by confocal scanning fluorescence microscopy. Fixed trophozoites treated with anti-IscS and anti-IscU antibodies displayed localized staining in small cellular structures distributed throughout the cytoplasm, including an accumulation of label around basal bodies and the base of flagellar axonemes (Fig. 3a; see also Fig. 4f). Figure 3a shows representative maximum projection images for both proteins merged with the corresponding differential interference contrast (DIC) images. The number of organelles detected per cell ranged from 25 to well over 100, as estimated by counting labelled structures in optical stacks of 300 nm thickness, suggesting a significant physiological role for this orga-

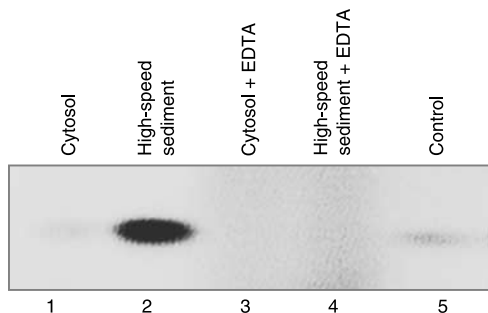


**Figure 2** Functional analysis of Fe-S protein maturation in *Giardia*. Incorporation of radioactive Fe-S clusters into recombinant apoferrdoxin was assayed as described in Methods. Assembly of the *de novo* synthesized Fe-S clusters into apoferrdoxin is observed exclusively when the high-speed sediment is used in the reaction. Ferrerdoxin maturation is inhibited by metal ion chelation with EDTA.

nelle in *Giardia*. Double labelling for IscS and IscU revealed that both proteins are present in the same intracellular compartment (Fig. 3b; see also Figs 4c, d), as would be expected from their functional partnership in Fe-S cluster biosynthesis. Interestingly, chaperonin Cpn60 was not found to colocalize with IscS in double labelling experiments (Fig. 3c), indicating that the current function of Cpn60 in *Giardia* is not conducted in the same compartment as Fe-S cluster biosynthesis. Unlike IscU, *Giardia* IscS lacks a recognizable putative mitochondrial targeting signal<sup>5</sup> but its clear compartmentalized localization suggests that organellar protein import mechanisms in *Giardia* are not solely dependent on N-terminal presequences. A similar observation was recently made in *Trachi-pleistophora*, where mtHsp70 is efficiently targeted into mito-

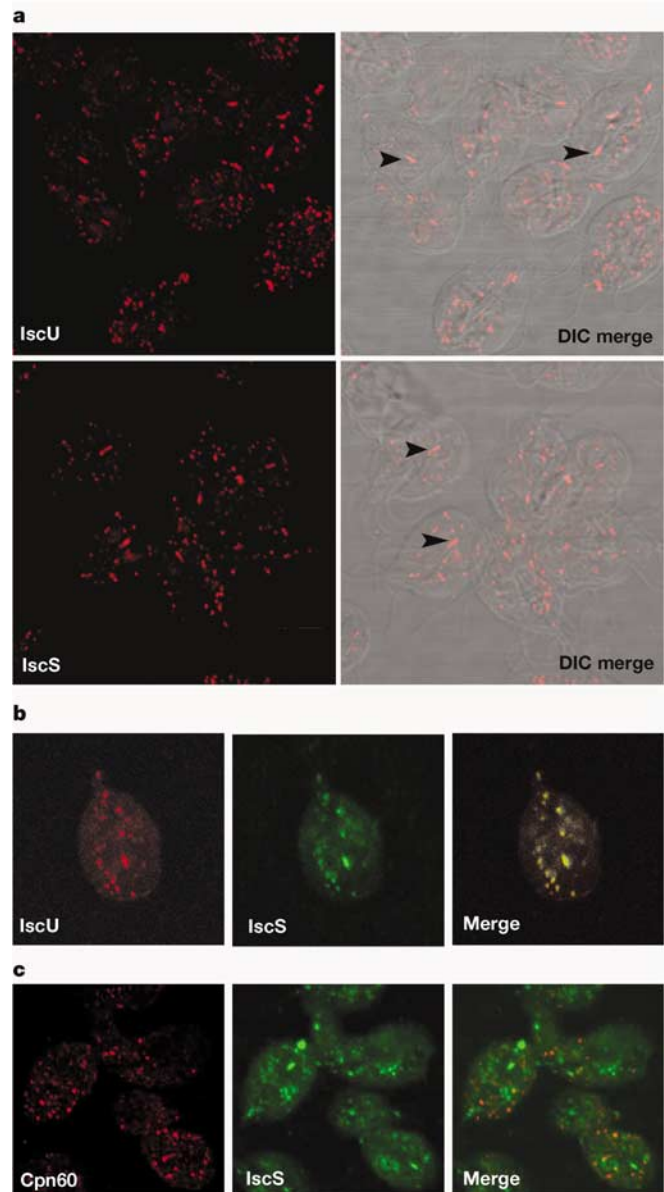


**Figure 3** Localization of IscS and IscU in *Giardia* trophozoites by confocal immunofluorescence microscopy. **a**, *Giardia* trophozoites, fixed and permeabilized as described in Methods, were probed independently with antibodies specific for IscU and IscS. The label is located in foci throughout the cytoplasm; distinctive accumulation is also observed around the base of flagellar axonemes and basal bodies (indicated by arrowheads). **b**, Double labelling of *Giardia* trophozoites with anti-IscS and anti-IscU antibodies; colocalization of label is readily apparent. **c**, Double labelling of trophozoites with anti-IscS and anti-Cpn60 antibodies; no colocalization of label is observed.

chondrial remnant organelles despite the absence of a recognizable organelle targeting presequence<sup>10</sup>.

We used immunoelectron microscopy to investigate the structure of the organelle harbouring the *Giardia* Isc proteins. Immunogold labelling of IscS and IscU was localized over small organelles bounded by two limiting membranes (Fig. 4a–d). Labelling densities for IscS and IscU were at least 200 and 110 fold higher than over cytosol or peripherally located endolysosomes respectively (Fig. 4i). Double labelling for IscS and IscU localized both of these antigens in the same class of double membrane-bounded structures (Fig. 4c, d), and similar structures were found in epoxy resin sections (Figs 4e–h). In cryosections, gold-labelled double-membrane-bounded organelles were elongated in profile and measured an average of 142 × 61 nm while in epoxy resin sections these structures measured an average of 137 × 68 nm (Fig. 4j). These organelles were found distributed throughout the cytosol and in close proximity to flagellar axonemes (Fig. 4f), in agreement with the distribution observed by confocal microscopy.

Immunogold labelling of Cpn60 did not produce significant signal over membrane-bounded structures (not shown), in agreement with a previous report on the lack of association of *Giardia* Cpn60 with biological membranes<sup>16</sup> and consistent with our confocal microscopy observations. The differential distribution of Cpn60 and IscS is noteworthy because the mitochondrial ancestry of both proteins is strongly supported by phylogenetic analyses.

However, the fact that only Isc proteins are associated with membrane-bounded organelles suggests that Cpn60 has been relocated from its original mitochondrial compartment as part of an ongoing process of reductive evolution. Alternatively, the possibility that *Giardia* Cpn60 might have been acquired by lateral transfer from a prokaryotic organism related to the mitochondrial endosymbiont cannot be excluded<sup>19,20</sup>. The precise nature of the Cpn60 aggregates that render the characteristic punctate distribution in *Giardia* remains to be elucidated.

Overall, our data provide direct physical evidence for the presence of mitochondrial remnant organelles (mitosomes) in *Giardia*, as postulated on the basis of previous phylogenetic and biochemical studies<sup>3–7,15,21</sup>. Mitochondrial remnant organelles have also been observed in other amitochondrial protists including the microsporidian *Trachipleistophora hominis*, the apicomplexan *Cryptosporidium parvum* and the entamoebid *Entamoeba histolytica*<sup>8–10,22</sup>. *Giardia* has traditionally been considered to be one of the earliest-branching eukaryotes, although the significance of its basal position in phylogenetic reconstructions has been disputed<sup>1,2,23</sup>. The identification of mitosomes in this organism places the endosymbiotic event that led to mitochondria firmly before the evolutionary divergence of the diplomonads.

Energy generation and recycling of resources are thought to have driven the original endosymbiotic event. Whether ATP generation in the heterotrophic mitochondrial endosymbiont involved aerobic

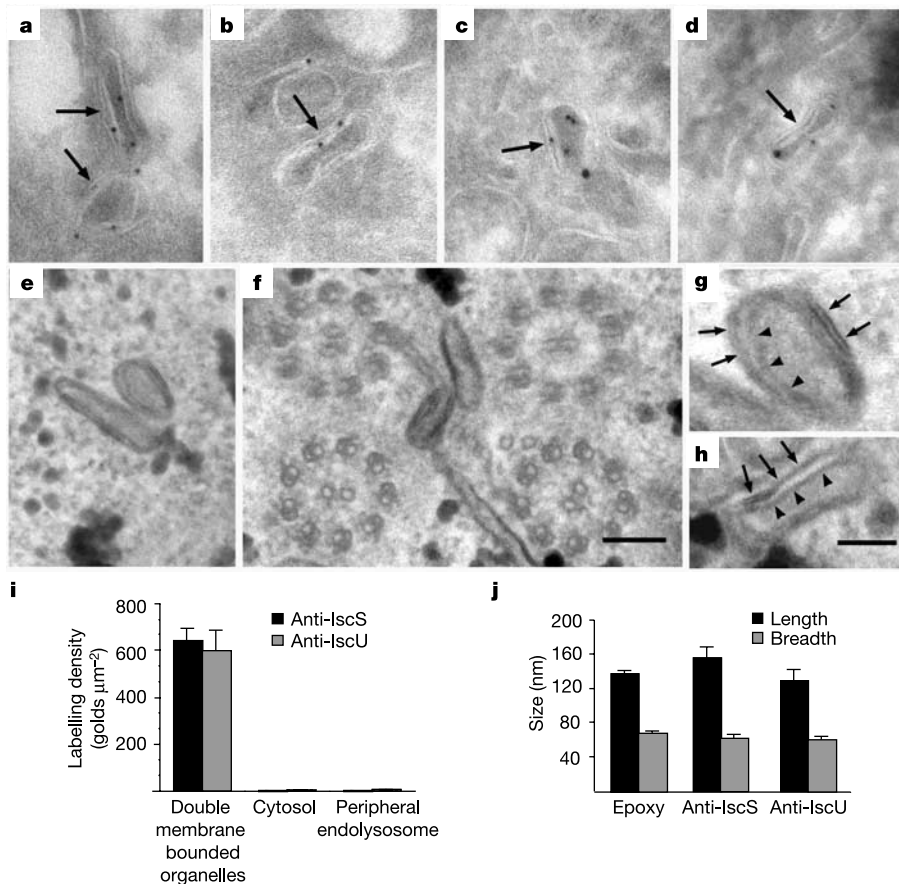


**Figure 4** Localization of IscS and IscU in *Giardia* trophozoites by transmission electron immunomicroscopy. **a–d**, Thawed frozen cryosections of glutaraldehyde-fixed *Giardia* were labelled with anti-IscS (**a**) and anti-IscU antibodies (**b**) or double-labelled (**c** and **d**) for anti-IscU (8 nm gold particles) followed by anti-IscS antibodies (12 nm gold particles). Arrows indicate double-membrane-bounded structures. Membranes appear as white profiles with this methodology. **e–h**, Epoxy resin sections of glutaraldehyde-fixed trophozoites. **f**, Double-membrane-bounded structures are shown in close proximity to flagellar axonemes. **g, h**, High-magnification images showing organelle double

membranes. Arrows point towards outer membranes while arrowheads identify inner membranes. **i**, Densities of labelling from typical labelling experiments were obtained as explained in Methods ( $n = 8$  for IscS and  $n = 7$  for IscU;  $n =$  number of scanned micrographs). **j**, Sizes of double membrane bounded organelles in epoxy resin and cryosections labelled with antibodies to either IscS or IscU ( $n = 43$  for epoxy resin,  $n = 13$  for IscS and  $n = 11$  for IscU;  $n =$  number of organelles). Intermembrane spacing in epoxy resin was  $9.36 \pm 0.49$  nm ( $n = 29$ ). Scale bars, 100 nm (**a–f**) and 50 nm (**g, h**).

or anaerobic respiration—as proposed by current theories of eukaryotic evolution (reviewed in ref. 24)—all electron transport chains and modes of heterotrophic oxidative metabolism share a common feature: several of their key enzymes rely on Fe–S centres for their catalytic activities (for example, ferredoxins, pyruvate:ferredoxin oxidoreductase, succinate dehydrogenase, cytochrome *b*-associated Rieske protein, aconitase, hydrogenase)<sup>12</sup>. Thus, the original endosymbiont must have possessed the capacity to synthesize Fe–S clusters and to assemble them into functional redox and electron transport proteins. These crucial metabolic functions could have secured the permanent establishment of the mitochondrial endosymbiont in the newly formed eukaryotic cell.

Our data also directly demonstrate an essential metabolic function for the mitochondria of amitochondriate protists. The apparent ubiquity of Fe–S cluster assembly proteins in the genomes of all amitochondriate protists sequenced until now (for example, *Encephalitozoon*<sup>25</sup>, *Giardia*<sup>26</sup>, *Cryptosporidium*<sup>27</sup>, *Entamoeba* ([http://www.sanger.ac.uk/Projects/E\\_histolytica/](http://www.sanger.ac.uk/Projects/E_histolytica/)), (<http://www.tigr.org/tdb/e2k1/ehal/>)) suggests that Fe–S cluster biosynthesis and Fe–S protein maturation might have been the only biochemical features of the mitochondrial endosymbiont essential for eukaryotic cell survival under conditions of oxygen deprivation. Interestingly, hydrogen production by *Giardia* has recently been detected under strict anaerobic conditions<sup>28</sup>. The possibility that this process might also occur in the double-membrane-bounded organelles described here awaits the unequivocal localization of hydrogenase in this organism. We suggest that the requirement for the assembly and maturation of Fe–S proteins may have provided, for hundreds of millions of years, the selective pressure required for the retention of the mitochondrial endosymbiont in both aerobic and anaerobic environments. □

**Methods**

**Gene cloning, protein expression and antibody generation**

The entire coding regions of the *Giardia iscS* and *iscU* genes were amplified by PCR using *Giardia* genomic DNA as template and the primer pairs 5'-TATTTTAAATGAGGTACC TGGACAACCAAGCCACTACG-3' / 5'-AGTGGTGTGAGTCGACTAGTCATGCTT CCACTCTATGCTC-3' and 5'-AATTCTAATGGATCCCAAGCCTTCAGCTCTCTA GCACT-3' / 5'-CAGGAGGCACCCGGGTCAAGAAGACTTTGATACCTGTATC-3' designed on the basis of partial sequences retrieved from the *Giardia* genome database<sup>26</sup>. These incorporated unique *KpnI* and *SalI* sites and *BamHI* and *XmaI* sites (italics) into *iscS* and *iscU* respectively. PCR products were cloned directionally into plasmid pQE-32 (Qiagen) and transformed into *E. coli* M15 [pREP4]. N-terminal His-tagged proteins were purified under denaturing conditions by affinity chromatography following the manufacturer's protocol (Qiagen) and used to generate rabbit polyclonal anti-*IscS* and anti-*IscU* antibodies (Lampire Biological Laboratories). Mouse polyclonal anti-Cpn60 antibodies were generated using recombinant Cpn60 protein from *E. histolytica* prepared as described<sup>9</sup>.

**Organism, cell fractionation and western blotting**

*Giardia intestinalis* (WB strain, ATCC No. 30957) was used throughout this study. Trophozoites were partially lysed to a maximum 50% cell lysis in isotonic buffer (0.2 M mannitol, 50 mM sucrose, 10 mM KCl, 1 mM EDTA, 10 mM HEPES pH 7.4 supplemented with 70 μM E64 and 0.75 μg ml<sup>-1</sup> leupeptin). A low-speed sediment fraction composed of cell debris and unbroken cells was obtained by centrifugation at 1,000g for 10 min at 4 °C. The supernatant was further centrifuged at 108,000g for 30 min. The resulting high-speed sediment was resuspended in isotonic buffer. The high-speed supernatant was used as the soluble cytosolic fraction. Equivalent protein aliquots (10 μg) were electrophoresed on 10% or 12.5% polyacrylamide gels for detection of *IscS* and *IscU* respectively. Proteins were electroblotted onto nitrocellulose membranes, blocked by incubation in 2% skimmed milk in PBS and probed with anti-*IscS* (1:1,000) or anti-*IscU* (1:750) antibodies for 1 h at room temperature. Membranes were further incubated with anti-rabbit IgG antibodies conjugated to peroxidase (1:25,000) for 1 h at room temperature. Blots were developed using an ECL detection system (Amersham Biosciences).

**Reconstitution of Fe–S clusters in vitro**

Trophozoites were mechanically disrupted and fractionated as described above. Fe–S cluster formation by cytosolic and high-speed sediment fractions was determined using recombinant apoferritin from *Trichomonas vaginalis* as a reporter protein. Recombinant ferredoxin was prepared as described<sup>29</sup>. The standard reaction mixture contained 30–100 μg protein of tested fraction, 7 μg of apo-ferredoxin, 20 mM HEPES, 0.2% Triton-X100, 250 mM saccharose, 50 μM ferrous ascorbate, 20 mM DTT, 25 μM L-cysteine and 10 μCi of <sup>35</sup>S-L-cysteine. To observe inhibition of the reaction, 5 mM EDTA was added to the reaction mixture before the incubation. In controls, the cell fractions

were omitted. Reactions proceeded in an anaerobic jar under atmosphere of 95% nitrogen and 5% hydrogen gas for 90 min at 25 °C. Samples were separated on a 15% non-denaturing polyacrylamide gel at 4 °C, followed by gel vacuum-drying and autoradiography.

**Immunofluorescence confocal microscopy**

*Giardia* trophozoites were fixed in 4% paraformaldehyde in PBS for 30 min at 37 °C and permeabilized with cold acetone or 0.2% Triton X-100 in PBS for 5 min. After blocking with 1% BSA in PBS, slides were incubated overnight with anti-*Isc* rabbit antibodies (1:200 dilution) and subsequently with secondary anti-rabbit IgG-TRITC conjugate (1:300 dilution) for 1 h at 37 °C. In *Isc* colocalization experiments, slides treated with anti-*IscU* antibodies were further incubated with 250 μl of purified rabbit IgG immunoglobulins (40 μg ml<sup>-1</sup>) for 1 h at 37 °C followed by incubation with FITC-conjugated anti-*IscS* antibodies (Fluoro Tag FITC Conjugation Kit, Sigma). Slides were mounted with anti-fade mounting medium (Vectashield) and observed under a laser scanning confocal microscope (Radiance 2100, Bio-Rad). Images were collected using Bio-Rad LaserSharp 2000 software and processed with Adobe PhotoShop 7.0.

**Immunoelectron microscopy**

Organisms were fixed in 0.5% glutaraldehyde or 4% paraformaldehyde/0.1% glutaraldehyde each in 0.2 M PIPES buffer pH 7.2 for 30 min at room temperature, washed in PBS and stored at 4 °C. Cells were pelleted and cryoprotected in 2.3 M sucrose in PBS and frozen on cryosectioning stubs in liquid nitrogen and cryosectioned on a Leica ultracycromicrotome at 50–100 nm. Thawed cryosections were labelled using rabbit antisera against *Isc* proteins followed by 8 nm protein A gold<sup>30</sup>, contrasted in methyl cellulose/uranyl acetate and observed in a JEOL 1200EX transmission electron microscope. For quantitation, elongated or round profiles with evidence of double membranes and measuring less than 110 nm minor diameters were photographed at a nominal magnification of 40,000. Micrographs were recorded on phosphoimaging plates (4,342 × 4,912 pixels) (DITABIS, Germany) and stored as TIFF files and further magnified in Adobe Photoshop 5.5. Square lattice grids with spacing of 25 nm, 250 nm and 125 nm were generated on screen and point counting was used to estimate areas of double membrane structures, cytosol and peripherally located endolysosomes respectively. Double labelling using 8 nm and 12 nm gold particles was carried out as described elsewhere<sup>30</sup>. Standard errors of ratio estimates were computed according to ref. 31.

Received 7 April; accepted 22 July 2003; doi:10.1038/nature01945.

1. Adam, R. D. Biology of *Giardia lamblia*. *Clin. Microbiol. Rev.* **14**, 447–475 (2001).
2. Sogin, M. L. & Silberman, J. D. Evolution of the protists and protistan parasites from the perspective of molecular systematics. *Int. J. Parasitol.* **28**, 11–20 (1998).
3. Hashimoto, T., Sánchez, L. B., Shirakura, T., Müller, M. & Hasegawa, M. Secondary absence of mitochondria in *Giardia lamblia* and *Trichomonas vaginalis* revealed by valyl-tRNA synthetase phylogeny. *Proc. Natl Acad. Sci. USA* **95**, 6860–6865 (1998).
4. Roger, A. J. *et al.* A mitochondrial-like chaperonin 60 gene in *Giardia lamblia*: evidence that diplomonads once harbored an endosymbiont related to the progenitor of mitochondria. *Proc. Natl Acad. Sci. USA* **95**, 229–234 (1998).
5. Tachezy, J., Sánchez, L. B. & Müller, M. Mitochondrial type iron-sulfur cluster assembly in the amitochondriate eukaryotes *Trichomonas vaginalis* and *Giardia intestinalis*, as indicated by the phylogeny of *IscS*. *Mol. Biol. Evol.* **18**, 1919–1928 (2001).
6. Morrison, H. G., Roger, A. J., Nystul, T. G., Gillin, F. D. & Sogin, M. L. *Giardia lamblia* expresses a proteobacterial-like DnaK homolog. *Mol. Biol. Evol.* **18**, 530–541 (2001).
7. Arisue, N., Sánchez, L. B., Weiss, L. M., Müller, M. & Hashimoto, T. Mitochondrial-type hsp70 genes of the amitochondriate protists *Giardia intestinalis*, *Entamoeba histolytica* and two microsporidians. *Parasitol. Int.* **51**, 9–16 (2002).
8. Mai, Z. *et al.* Hsp60 is targeted to a cryptic mitochondrion-derived organelle (“crypton”) in the microaerophilic protozoan parasite *Entamoeba histolytica*. *Mol. Cell. Biol.* **19**, 2198–2205 (1999).
9. Tovar, J., Fischer, A. & Clark, C. G. The mitosome, a novel organelle related to mitochondria in the amitochondrial parasite *Entamoeba histolytica*. *Mol. Microbiol.* **32**, 1013–1021 (1999).
10. Williams, B. A. P., Hirt, R. P., Lucocq, J. M. & Embley, T. M. A mitochondrial remnant in the microsporidian *Trachipleistophora hominis*. *Nature* **418**, 865–869 (2002).
11. Lill, R. & Kispal, G. Maturation of cellular Fe-S proteins: an essential function of mitochondria. *Trends Biochem. Sci.* **25**, 352–356 (2000).
12. Müller, M. in *Molecular Medical Parasitology* (eds Marr, J., Nilsen, T. & Komuniecki, R.) 125–139 (Academic, London, 2003).
13. Dyall, S. D. & Johnson, P. J. Origins of hydrogenosomes and mitochondria: evolution and organelle biogenesis. *Curr. Opin. Microbiol.* **3**, 404–411 (2000).
14. Embley, T. M., van der Giezen, M., Horner, D. S., Dyal, P. L. & Foster, P. Mitochondria and hydrogenosomes are two forms of the same fundamental organelle. *Phil. Trans. R. Soc. Lond.* **358**, 191–203 (2003).
15. Lloyd, D. & Harris, J. C. *Giardia*: highly evolved parasite or early branching eukaryote? *Trends Microbiol.* **10**, 122–127 (2002).
16. Soltys, B. J. & Gupta, R. S. Presence and cellular distribution of a 60-kDa protein related to mitochondrial hsp60 in *Giardia lamblia*. *J. Parasitol.* **80**, 580–590 (1994).
17. Tokumoto, U. *et al.* Network of protein-protein interactions among iron-sulfur cluster assembly proteins in *Escherichia coli*. *J. Biochem. (Tokyo)* **131**, 713–719 (2002).
18. Tong, W. H. & Rouault, T. Distinct iron-sulfur cluster assembly complexes exist in the cytosol and mitochondria of human cells. *EMBO J.* **19**, 5692–5700 (2000).
19. Andersson, J. O., Sjogren, A. M., Davis, L. A., Embley, T. M. & Roger, A. J. Phylogenetic analyses of diplomonad genes reveal frequent lateral gene transfers affecting eukaryotes. *Curr. Biol.* **13**, 94–104 (2003).
20. Doolittle, W. F. You are what you eat: a gene transfer ratchet could account for bacterial genes in eukaryotic nuclear genomes. *Trends Genet.* **14**, 307–311 (1998).
21. Lloyd, D. *et al.* The ‘primitive’ microaerophile *Giardia intestinalis* (syn. *lamblia*, *duodenalis*) has

- specialized membranes with electron transport and membrane-potential-generating functions. *Microbiology* **148**, 1349–1354 (2002).
22. Riordan, C. E., Ault, J. G., Langreth, S. G. & Keithly, J. S. *Cryptosporidium parvum* Cpn60 targets a relict organelle. *Curr. Genet. advance online publication*, 20 August 2003 (doi:10.1007/s00294-003-0432-1).
  23. Philippe, H. et al. Early-branching or fast-evolving eukaryotes? An answer based on slowly evolving positions. *Proc. R. Soc. Lond. B* **267**, 1213–1221 (2000).
  24. Martin, W., Hoffmeister, M., Rotte, C. & Henze, K. An overview of endosymbiotic models for the origins of eukaryotes, their ATP-producing organelles (mitochondria and hydrogenosomes), and their heterotrophic lifestyle. *Biol. Chem.* **382**, 1521–1539 (2001).
  25. Katinka, M. D. et al. Genome sequence and gene compaction of the eukaryote parasite *Encephalitozoon cuniculi*. *Nature* **414**, 450–453 (2001).
  26. McArthur, A. G. et al. The *Giardia* genome project database. *FEMS Microbiol. Lett.* **189**, 271–273 (2000).
  27. Strong, W. B. & Nelson, R. G. Preliminary profile of the *Cryptosporidium parvum* genome: an expressed sequence tag and genome survey sequence analysis. *Mol. Biochem. Parasitol.* **107**, 1–32 (2000).
  28. Lloyd, D., Ralphs, J. R. & Harris, J. C. *Giardia intestinalis*, a eukaryote without hydrogenosomes, produces hydrogen. *Microbiology* **148**, 727–733 (2002).
  29. Vidakovic, M. S., Fraczekiewicz, G. & Germanas, J. P. Expression and spectroscopic characterization of the hydrogenosomal [2Fe-2S] ferredoxin from the protozoan *Trichomonas vaginalis*. *J. Biol. Chem.* **271**, 14734–14739 (1996).
  30. Prescott, A. R., Lucocq, J. M., James, J., Lister, J. M. & Ponnambalam, S. Distinct compartmentalization of TGN46 and beta 1,4-galactosyl transferase in HeLa cells. *Eur. J. Cell Biol.* **72**, 238–246 (1997).
  31. Cochran, W. G. *Sampling Techniques* (John Wiley and Sons, London, 1977).

**Acknowledgements** We thank G. Clark, J. Bowyer and S. Cutting for critically reading the manuscript. A recombinant plasmid containing the *T. vaginalis* ferredoxin gene was provided by J. P. Germanas and K. Krause. The use of partial genome sequence information from the *Giardia* Genome Project Database<sup>26</sup> is acknowledged. The technical assistance of J. James and N. Somerville is also acknowledged. M.H. is a sabbatical visitor supported by CINVESTAV, México. Research at the Rockefeller University (gene cloning, antibody generation) was supported by a NIH grant to M.M. Research at Charles University (*in vitro* assembly of Fe-S clusters) was supported by a grant from FIRCA to J.Tachezy. J.M.L. (electron microscopy) was supported by a Research Leave Fellowship from the Wellcome Trust and by Tenovus Scotland. Research at Royal Holloway (bioinformatics, cell fractionation, fluorescence confocal microscopy, manuscript writing, project coordination) was supported by a Wellcome Trust grant to J.Tovar.

**Competing interests statement** The authors declare that they have no competing financial interests.

**Correspondence** and requests for materials should be addressed to J.Tovar (j.tovar@rhul.ac.uk). The sequence of *GlscU* has been deposited with GenBank under accession number AY040612.

## Allele substitution at a flower colour locus produces a pollinator shift in monkeyflowers

H. D. Bradshaw Jr<sup>1</sup> & Douglas W. Schemske<sup>2</sup>

<sup>1</sup>Department of Biology, University of Washington, Seattle, Washington 98195, USA

<sup>2</sup>Department of Plant Biology, Michigan State University, East Lansing, Michigan 48824, and W. K. Kellogg Biological Station, Hickory Corners, Michigan 49060, USA

The role of major mutations in adaptive evolution has been debated for more than a century<sup>1,2</sup>. The classical view is that adaptive mutations are nearly infinite in number with infinitesimally small phenotypic effect<sup>3</sup>, but recent theory suggests otherwise<sup>4</sup>. To provide empirical estimates of the magnitude of adaptive mutations in wild plants, we conducted field studies to determine the adaptive value of alternative alleles at a single locus, *YELLOW UPPER*<sup>5–7</sup> (*YUP*). *YUP* controls the presence or absence of yellow carotenoid pigments in the petals of pink-flowered *Mimulus lewisii*, which is pollinated by bumblebees<sup>5,8–10</sup>, and its red-flowered sister species<sup>11</sup> *M. cardinalis*, which is pollinated by hummingbirds<sup>5,8–10</sup>. We bred near-isogenic lines (NILs) in which the *YUP* allele from each species was substituted into the

other. *M. cardinalis* NILs with the *M. lewisii* *YUP* allele had dark pink flowers and received 74-fold more bee visits than the wild type, whereas *M. lewisii* NILs with the *M. cardinalis* *yup* allele had yellow-orange flowers and received 68-fold more hummingbird visits than the wild type. These results indicate that an adaptive shift in pollinator preference may be initiated by a single major mutation.

Where their ranges overlap, the monkeyflowers *M. lewisii* and *M. cardinalis* are >99% reproductively isolated by the difference in their pollinator guilds<sup>8,9</sup>. In previous studies of artificial F<sub>2</sub> hybrids between *M. lewisii* and *M. cardinalis*, we showed that flower colour has marked effects on pollinator visitation<sup>8</sup>, and that yellow pigment concentration is controlled in part by the major quantitative trait locus (QTL; reviewed in ref. 12), *YUP*<sup>6,7</sup>. Although F<sub>2</sub> populations are useful for mapping QTLs controlling differences in floral traits between species<sup>6,7,13</sup>, they are less than ideal for assessing the adaptive effect of a single mutation. The many intermediate flower phenotypes in an F<sub>2</sub> population<sup>6–8,13</sup> may provide a bridge for pollinators to develop learned visitation patterns completely unlike those that would occur as a result of a single-locus mutational step in an adaptive walk.

By substituting one allele for another using repeated backcrosses, NILs more closely mimic the effect of a single mutation likely to be part of an adaptive pollinator shift; that is, from bumblebee-pollinated to hummingbird-pollinated, or vice versa. The dominant *M. lewisii* *YUP* allele prevents carotenoid deposition, so the petals show only their pink anthocyanin pigments. The recessive *M. cardinalis* *yup* allele allows carotenoid deposition in the petals and produces red flowers when present in conjunction with a high concentration of anthocyanins<sup>5–7</sup>. Although phylogenetic evidence suggests that the hummingbird pollination syndrome of *M. cardinalis* is derived from a bee-pollinated ancestor similar to *M. lewisii*<sup>11</sup>, we constructed *YUP* NILs in both species (Fig. 1). The wild-type *M. lewisii* NIL is pink-flowered (Fig. 1a), whereas the ‘mutant’ NIL homozygous for the introgressed *M. cardinalis* *yup* allele has pale yellow-orange flowers (Fig. 1b). The wild-type *M. cardinalis* NIL is red-flowered (Fig. 1c), but the presence of a dominant *M. lewisii* *YUP* allele produces a dark-pink-flowered NIL (Fig. 1d).

Pollinator visitation rates were determined by field observation of NIL experimental arrays near a zone of sympatry between *M. lewisii* and *M. cardinalis*<sup>5,8</sup> to ensure that pollinators were familiar with both species in their natural habitat. Bumblebees strongly prefer pink-flowered NILs carrying the *YUP* allele (Fig. 1a, d) in both the *M. lewisii* and *M. cardinalis* genetic backgrounds (Table 1). Hummingbirds prefer yellow-orange- or red-flowered NILs homozygous for the *yup* allele (Fig. 1b, c) in both backgrounds (Table 1).

The striking effect of flower colour on pollinator specificity is evidence for the adaptation of both monkeyflower species to their current pollinators (Table 1). A wild-type pink *M. lewisii* flower (Fig. 1a) is >700 times more likely to be visited by a bumblebee than by a hummingbird, whereas the yellow-orange-flowered ‘mutant’ (Fig. 1b) is only 1.8 times as likely to be visited by a bumblebee. In the *M. cardinalis* background, a wild-type red flower (Fig. 1c) is >1,200 times more likely to be visited by a hummingbird than by a bumblebee, but the pink-flowered ‘mutant’ (Fig. 1d) is visited only 15 times as frequently by hummingbirds.

When these visitation rates are compared with the results from our previous F<sub>2</sub> QTL mapping population<sup>8</sup>, we find that the F<sub>2</sub> experiments accurately predict pollinator visitation when we consider only bumblebees visiting *M. lewisii* NILs, and hummingbirds visiting *M. cardinalis* NILs. In *M. lewisii* NILs and the F<sub>2</sub>, the wild-type pink flowers were visited by bumblebees at about a fivefold higher rate than were the ‘mutant’ yellow-orange flowers (Table 1 and ref. 8). In *M. cardinalis* NILs, hummingbirds showed a slight 1.1-fold preference for wild-type red flowers over the pink-flowered ‘mutants’, similar to that found in the F<sub>2</sub> population (Table 1 and ref. 8). The close correspondence of the results from these indepen-